Journal of Structural Geology, Vol. 12, No. 7, pp. 883 to 894, 1990
Printed in Great Britain

0191-8141/90 $03.00+0.00
Pergamon Press plc

Microfractures and their role in deformation of a quartz arenite from the central Appalachian foreland

CHARLES M. ONASCH

Department of Geology, Bowling Green State University, Bowling Green, OH 43403, U.S.A.

(*Received* 6 *October* 1989; *accepted in revised form* 20 *February* 1990)

Abstract—Microfractures are pervasive in the Massanutten Sandstone, a quartz arenite exposed in a doubly-plunging synclinorium in the central Appalachian foreland. They are present as fluid inclusion planes (FIPS) and microveins parallel the FIPS. FIPS occur in three orthogonal sets: horizontal; vertical and normal to the fold axis; and vertical and parallel to the fold axis. The geometry, distribution and age of FIPS relative to other microstructures shows that microfractures developed during folding. Microfracturing followed layer-parallel shortening by dislocation flow and was coeval with the peak of pressure solution that marked the final stages of folding.

Microfracture densities are extremely high (>160 mm^{-1}) in many samples. Rapid closure of microfractures suppressed brecciation and prevented microfractures from propagating unstably to form joints.

Microfracture opening accounts for significant finite strain with extensional strains of up to 11.1% and associated volume increases of over 16.0%. The general lack of shortening microstructures indicates that a net volume increase is likely and that the Massanutten Sandstone may have served as a sink for dissolved phases from adjacent units undergoing volume-loss deformation.

INTRODUCTION

MICROFRACTURES are a common structure in many deformed rocks. They are important in process zones of major joints (Friedman *et al.* 1972) and are a precursor to shear failure (Scholz 1968b, Engelder 1974). In foreland regions, microfracturing is an important deformation mechanism, especially in sandstones (Narahara & Wiltschko 1986, Mitra 1987). Microfractures have proven useful in a number of applications such as the study of stress directions (Wise 1964, Gallagher *et al.* 1974, Simmons & Richter 1976, Wang & Simmons 1978, Dula 1981, Haimson & Doe 1983, Kranz 1983, Plumb *et al.* 1984, Pêcher *et al.* 1985, Lespinasse & Pêcher 1986, Kowallis *et al.* 1987, Laubach 1989). Closed microfractures have been used to provide information about the thermal history during deformation (Sprunt & Nur 1976, Kowallis *et al.* 1987).

Despite the widespread recognition and use of microfractures, little is known about: (1) their role during folding; (2) their temporal and spatial relationship to other microstructures; and (3) the possibility that pervasive microfracturing could contribute significantly to the finite strain and result in a volume-gain deformation. The purpose of this study is to address these questions with an analysis of microfractures in a deformed quartz arenite from the central Appalachian foreland.

Geologic setting

Microfractures were examined in the Lower Silurian Massanutten Sandstone of the Appalachian Great Valley province (Fig. 1). The Massanutten Sandstone consists of 250 m of interbedded sandstone and conglomerate with quartz comprising over 90% of the framework grains and cement.

The Massanutten Sandstone is exposed in two NE-trending, doubly-plunging synclinoria (Figs. 1 and 2), collectively known as the Massanutten synclinorium (Allen 1967, Rader & Biggs 1976). In most places, this structure has a moderately-dipping northwest limb and a steep to overturned southeast limb (Fig. 2). Locally, the northwest limb is also overturned producing a peculiar 'omega' structure in cross-section. The synclinorium is rootless and is part of the Blue Ridge thrust sheet (Fig. 2) which, together with the underlying North Mountain sheet, was transported northwestward some 65 km during the Alleghanian Orogeny (Evans 1989). Folding in the Massanutten synclinorium resulted from shortening

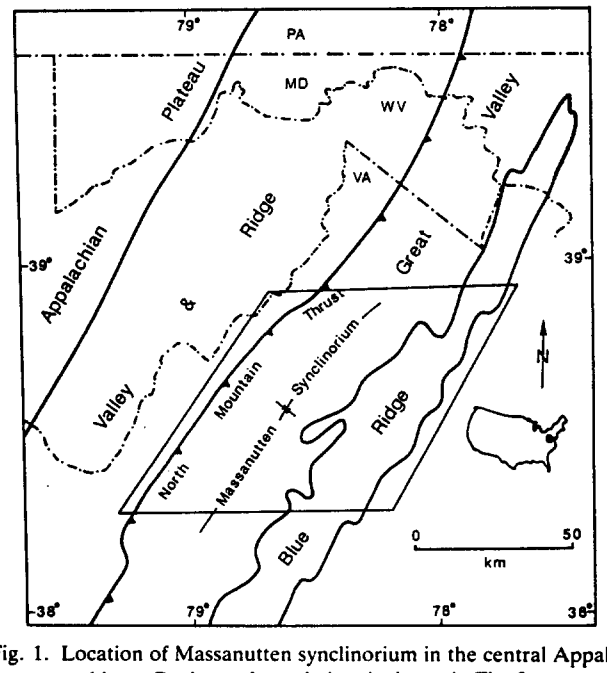

Fig. 1. Location of Massanutten synclinorium in the central Appalachians. Geology of area in box is shown in Fig. 2.

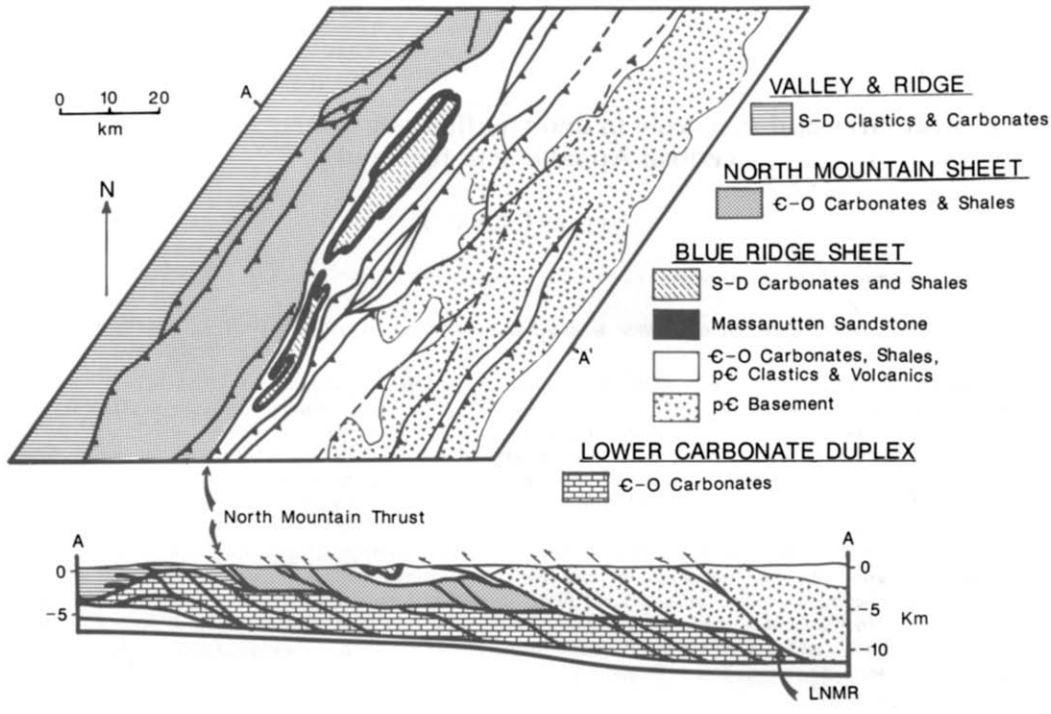

Fig. 2. Geologic map and cross-section showing location of Massanutten Sandstone relative to major thrust sheets and autochthonous rocks of the region. LNMR—Lower North Mountain ramp. Map and cross-section are modified from Evans (1989).

in the Blue Ridge sheet during transport and movement of the sheet over the upper North Mountain thrust ramp (Evans 1989).

Samples of the Massanutten Sandstone were taken at 47 localities around the Massanutten synclinorium, including both limb and hinge areas (Figs. 3 and 4). A previous study (Onasch 1984) proposed that the Massanutten synclinorium developed by buckling and that the Massanutten Sandstone behaved as a single stiff layer. Evidence for a neutral surface within the sandstone is preserved in extreme outer arc portions of the hinge. In order to determine if microfracture development changed as a function of position relative to the neutral surface, sample traverses were made across the entire thickness of the unit at four locations (Figs. 3 and 4).

NATURE OF MICROFRACTURES IN THE MASSANUTTEN SANDSTONE

Both open and closed microfractures occur in the Massanutten Sandstone. Closed microfractures occur either as fluid inclusion planes (FIPS) or microveins. Open microfractures are comparatively rare and will not be discussed in this paper.

Fluid inclusion planes are closed, intragranular or transgranular microfractures, 1–5 μm wide, decorated by bubbles or fluid inclusions. The inclusions were trapped when the microfracture was healed by local-scale diffusive mass transfer or sealed by precipitation of material transported from distances greater than grain scale (Smith & Evans 1984). FIPS are synonymous with Tuttle lamellae (Hobbs *et al.* 1976, Mitra 1987, Groshong 1988), bubble trails (Engelder 1984), bubble planes (Simmons & Richter 1976, Kowallis *et al.* 1987), and fluid inclusion trails (Lespinasse & Pêcher 1986).

Microveins are closed, transgranular microfractures that range in width between arbitrarily-defined lower and upper limits of 10 and 200 μm, respectively. Microveins are much thinner than macroscopic veins which can be recognized in hand sample. Macroscopic veins are rare in Massanutten Sandstone.

Fluid inclusion planes

Of the two types of closed microfractures, FIPS are most common (Fig. 5a). Over 75% of the microfractures observed in the Massanutten Sandstone are closed and contain fluid-filled inclusions. The inclusions decorating the planes are spherical to subspherical and range in diameter from less than 1 μm to 5 μm (Fig. 5b). The inclusions are generally two-phase with liquid and vapor present (Fig. 5b). Both transgranular and intragranular FIPS occur in the Massanutten Sandstone. The latter are more common where clay matrix or iron oxide grain coatings are present (Fig. 5c). Transgranular FIPS are favored where quartz grains are surrounded by quartz cement and impurities such as clay are lacking. No offset was observed where FIPS cross pre-existing features (Fig. 5a) indicating that FIPS originated as Mode I cracks.

The spacing index of FIPS (Table 1) ranges from less than 5 mm^{-1} in samples with few FIPS (Fig. 5a) to 168 mm^{-1} in samples with profuse FIPS (Figs. 5d & e). Transgranular FIPS tend to have higher densities than intragranular FIPS. The highest densities observed are several times greater than microfracture densities pre-

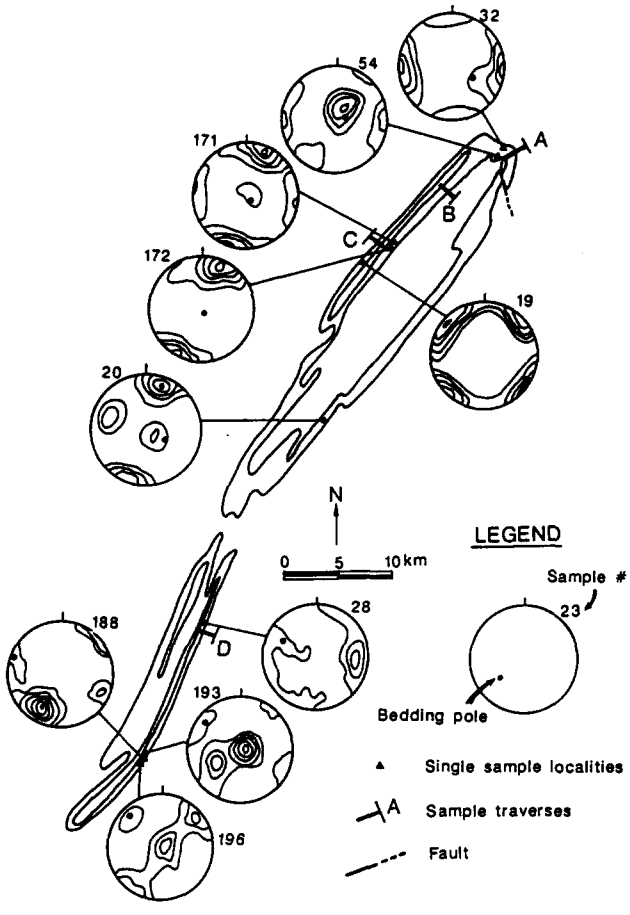

Fig. 3. Geologic map of the Massanutten Sandstone showing single sample stations and multiple sample traverses (A–D) of Fig. 4. Contoured equal-area plots are poles to FIPS at single sample stations. Contour interval is 3-sigma and *n* for each plot is 150–175.

viously reported for either naturally or experimentally deformed rocks (see Blenkinsop & Rutter 1986).

Microveins

Microveins are present in most samples, but in smaller numbers than FIPS. They are parallel to the FIPS (Fig. 5c) and do not offset pre-existing features. Hence, they also originated as Mode I cracks.

The quartz filling microveins is in optical continuity with wall rock grains (Figs. 6a & b) making microveins difficult or impossible to see in either plane or polarized light. In samples with high fluid inclusion densities, microveins are visible in plane light as transgranular zones that are relatively free of inclusions (Fig. 6a). The most reliable method for studying microveins proved to be cathodoluminescence (Fig. 6c) where they are clearly visible as reddish-brown luminescing tabular zones traversing detrital grains that luminesce either brown or blue.

The luminescent color of quartz is affected by the temperature at the time of formation (Sprunt & Nur 1979, Marshall 1988). The dull reddish-brown luminescence of the microvein fill is typical of slow, relatively defect-free growth of quartz at low temperatures (Marshall 1988). The similarity in color between the microvein fill and diagenetic pore-filling cement (Fig. 6c) indicates that the temperature during microfracturing was similar to that during diagenesis. Based on illite crystallinity in shales of the underlying Martinsburg Formation, the maximum temperature is estimated to have been 180–200°C (Epstein 1988).

The lack of FIPS within most microveins is evidence that microveins are generally younger. However, some microveins either contain or are cross-cut at low angles by FIPS indicating that they are in part coeval.

ORIENTATION AND DISTRIBUTION OF FLUID INCLUSION PLANES

FIP orientations were determined using a universal stage microscope. Three mutually-perpendicular sections were examined for every sample. Between 50 and 75 orientation measurements were made on each section. Data from the three sections were rotated into their true orientation, plotted together on an equal-area stereonet and contoured using the Kamb (1959) method (Figs. 3 and 4). Because microveins are parallel to FIPS, statements in the following sections about FIP orientations and occurrences also apply to microveins.

FIPS in the Massanutten Sandstone tend to occur in three orthogonal sets (Fig. 7): (1) horizontal (set I); (2) vertical and normal to the axis of the Massanutten synclinorium (set II); and (3) vertical and parallel to the axis (set III). Most samples have one or two of these sets and some have additional maxima as well (Figs. 3 and 4).

The distribution of the three orthogonal sets or combination of sets across the study area was determined by classifying each sample according to the set(s) present. A sample was said to contain a particular set if any portion of the area(s) bounded by the 6-sigma contour for the sample plot (Figs. 3 and 4) fell within the 4-sigma contour of the composite plot of all samples (Fig. 7). The 6-sigma contour level was chosen to enhance the statistical significance.

Using this criterion, all samples contain at least one of the orthogonal sets (Fig. 8a). Samples with two sets are slightly more common than those with just one, and samples with all three are comparatively rare (Fig 8a). Set II is most common, whether occurring alone or in combination with other sets (Fig. 8b).

The orientation of the three orthogonal sets bears a symmetrical relationship to the geometry of the Massanutten synclinorium. Geometric relationships such as these are common (e.g. Stearns 1968) and can be explained by fracturing during folding (Ramsay & Huber 1987). A uniform pattern of microfractures that lacks a geometric relationship to regional structures would be evidence for development of microfractures after folding. This is the case in the Washington, D.C., area, 120 km to the east, where microfractures have a consistent 320° strike and are non-symmetrical to local and regional folds (Tuttle 1949). In the Massanutten synclinorium, coeval microfracturing and folding is supported by the geometrical relationship between microfractures and the synclinorium and by the age relations

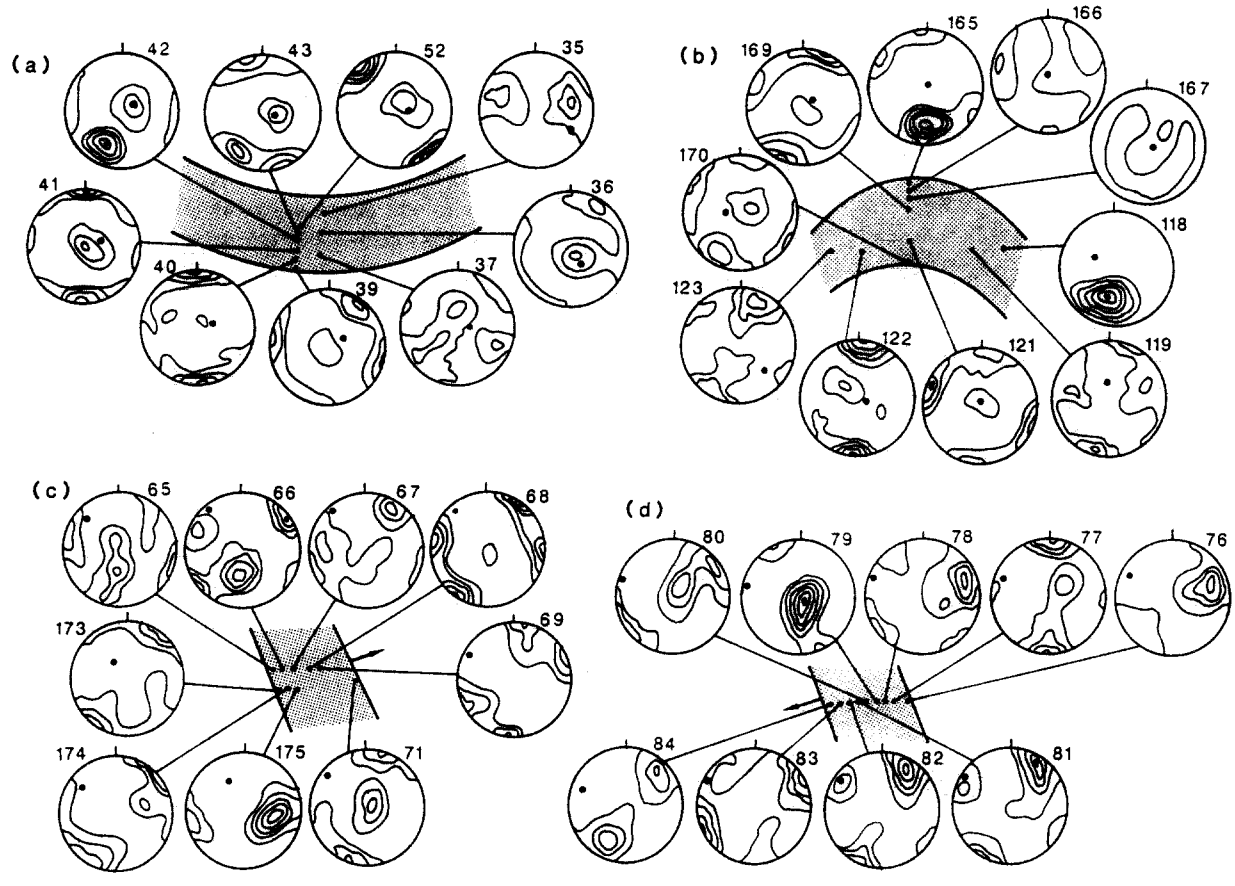

Fig. 4. Contoured equal-area plots of poles to FIPS for samples from traverses A–D shown on Fig. 3. Sample locations for each traverse are shown in schematic, strike-normal cross-sections of Massanutten Sandstone (stippled). Northwest on each section is to left. Arrows on bedding in sections C and D are younging direction. Contour interval is 3-sigma and n for each plot is 150–175.

between microfractures and other microstructures whose role in folding is well documented.

Relationship of microfractures to other microstructures

Deformation of the Massanutten Sandstone occurred by several mechanisms including dislocation flow, microfracturing, pressure solution and possibly grain-boundary sliding (Onasch 1987). Although the relative importance of each mechanism varies around the synclinorium, their relative ages do not change.

Deformation lamellae, undulose extinction and subgrains are the earliest microstructures and are the product of dislocation flow. The lamellae record predominantly NW–SE layer-parallel shortening that preceded or accompanied the early stages of buckling (Onasch 1984, 1987). Some samples in extreme outer arc hinge positions also show evidence for layer-parallel extension during buckling (Onasch 1984). FIPS cut deformation lamellae (Fig. 6e), and so post-date dislocation flow.

Pressure-solution features such as seams of insoluble residue (Fig. 6f), sutured grain boundaries (Fig. 5c) and syntaxial overgrowths (Fig. 6c) are common in portions of the Massanutten Sandstone, especially where clay matrix is present. The relatively inclusion-free zones rimming grains in Fig. 5(e) are also believed related to pressure solution in a form of diffusion-accommodated grain-boundary sliding.

Cross-cutting relations between microfractures and pressure-solution features are ambiguous suggesting that they were contemporaneous. Solution seams truncate against or are offset across microveins (Fig. 6f). The simple explanation is that the seams are younger; however, the seam could have acted as an elastic discontinuity which stopped microvein propagation in which case the microveins are younger. In some microveins which are not offset across seams, insoluble material can be traced undisturbed through the microvein indicating that the seam is younger. The FIPS and microveins are normal to the solution seams which shows that they could have formed at the same time. Because pressure solution is thought to have occurred during the final stages of fold tightening (Onasch 1987), microfracturing is contemporaneous with folding.

Role of fluid inclusion planes during folding

The relative age of the three FIP sets and their irregular development in the synclinorium (Fig. 9) also support the interpretation that they formed during folding. From oldest to youngest, the most common sequence is: set II; set III; and set I. In some hinge samples (e.g. MS-54, Fig. 3), set I is older than one or both of the other sets. The variation in relative age may indicate that set I developed in response to different causes in the hinge as compared to the limbs. In the hinge, the

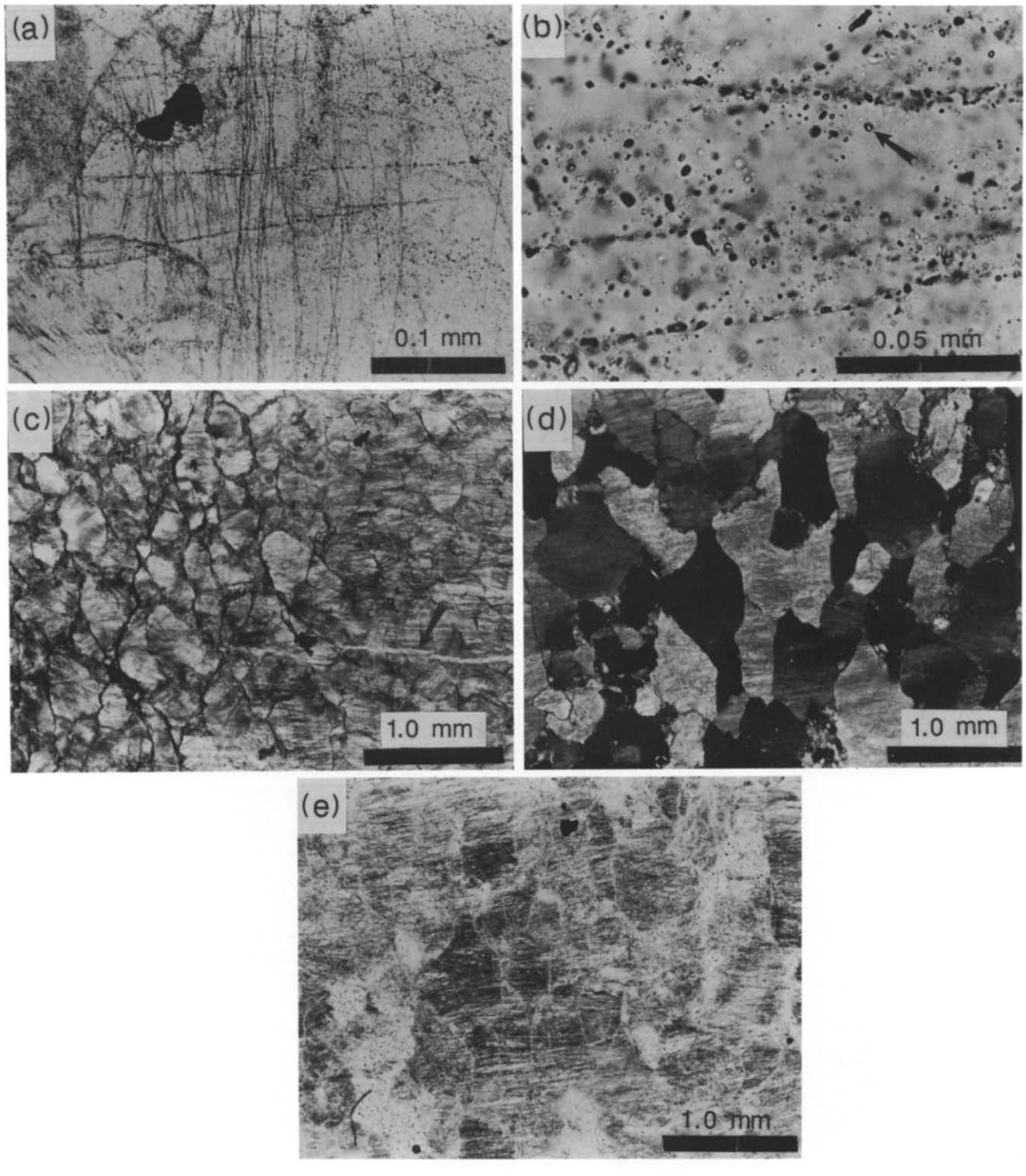

Fig. 5. Photomicrographs of FIPS in Massanutten Sandstone. (a) Orthogonal sets of FIPS. Note lack of offset at FIP intersections. (b) Inclusions defining planes. Vapor bubble is evident within inclusion indicated by arrow. (c) Effects of variable clay matrix on development of FIPS. Area on left has clay matrix, shows effects of considerable pressure solution, and has sparse, intragranular FIPS. Area to right has no clay matrix, shows little evidence for pressure solution, and has abundant transgranular FIPS. Arrow indicates microvein parallel to FIPS. (d) Profuse development of FIPS with obvious elongation of grains normal to FIPS; polarized light. (e) Plane light view of (d). Relatively inclusion-free rims around many grains may be result of diffusion-accommodated grain-boundary sliding.

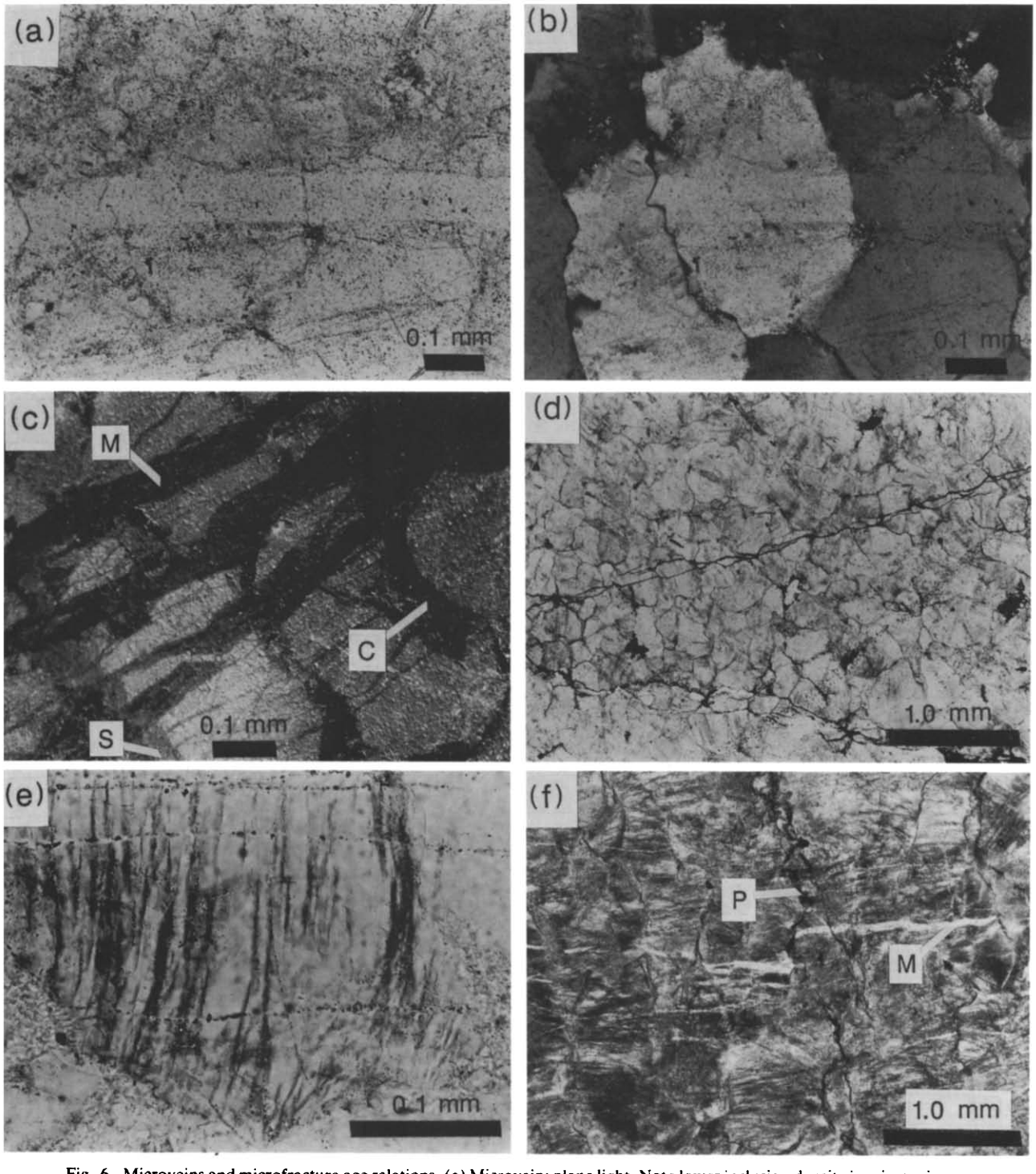

Fig. 6. Microveins and microfracture age relations. (a) Microvein; plane light. Note lower inclusion density in microvein as compared to wall rock. (b) Polarized light view of (a) showing optical continuity between vein fill and wall rock grains. (c) Cathodoluminescence photomicrograph of microvein network (M). Note that luminescence of microvein fill is same as pore-filling cement (C). Lighter syntaxial overgrowths (S) seen along grain boundaries are believed to result from solution-deposition during deformation. (d) Two directions of open microfractures. (e) FIPS (horizontal) cutting deformation lamellae (vertical). (f) Cross-cutting relations between FIPS, pressure-solution seams (P) and Microveins (M).

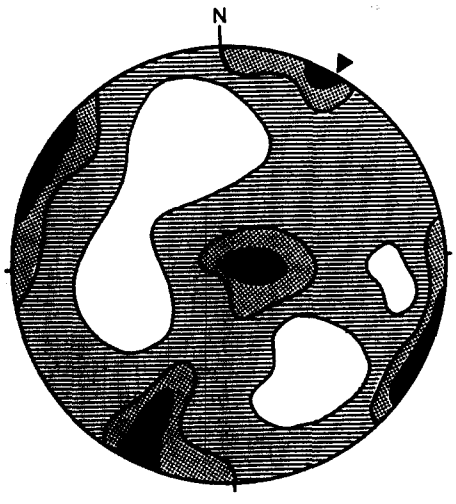

Fig. 7. Composite plot of 7525 FIPS. Contour interval is 2-sigma. Trend of Massanutten synclinorium indicated with arrow. Note three orthogonal sets: horizontal (set I); normal to fold axis (set II); and parallel to fold axis (set III).

bedding-parallel orientation and relative timing are consistent with set I having developed during layer-parallel shortening after dislocation flow. In contrast, set I in the limbs is at a high angle to bedding, is extensively developed in the overturned southeast limb (Fig. 9a), and is very common in the more steeply-dipping segments of the northwestern limb (e.g. MS-71, Fig 4). Such a geometry and timing is consistent with set I having formed in response to layer-parallel extension during the latter stages of folding in overturned or steeply-dipping limbs (Price 1967, Berger *et al.* 1979).

The roles of sets II and III FIPS in folding are not clear. Set II is parallel to the NW–SE compression that was responsible for the thrusting and macrofolding in the region. Although parallel to this compression, their orientation is not compatible with the stress system associated with foreland deformation. With thrusting, the minimum principal stress would be vertical (Anderson 1951) and resulting extension fractures would be horizontal. Cross-fold extension fractures, such as set II FIPS, are common in the Appalachian foreland (Engelder & Geiser 1980), yet they cannot be a direct product of the stresses related to thrusting (Srivastava & Engelder 1990). This paradox can be resolved by strike-parallel stretching that results from the arcuate shape of the thrust belt or by the presence of lateral ramps (Srivastava & Engelder 1990).

If set II FIPS are associated with strike-parallel stretching during thrusting and related folding, they could have formed over a long span of time. This may account for their relative abundance in all locations (Fig. 8b). Because they are normal to the fold axis, their orientation would be unchanged by subsequent folding. Thus, their attitude relative to bedding cannot be used as an indication of their timing during folding. However, set II is consistently the oldest set, except locally in the hinge, which indicates that it may have formed during the early stages of folding.

Set III cannot be a product of the regional NW–SE shortening; therefore, it must be related to local stress

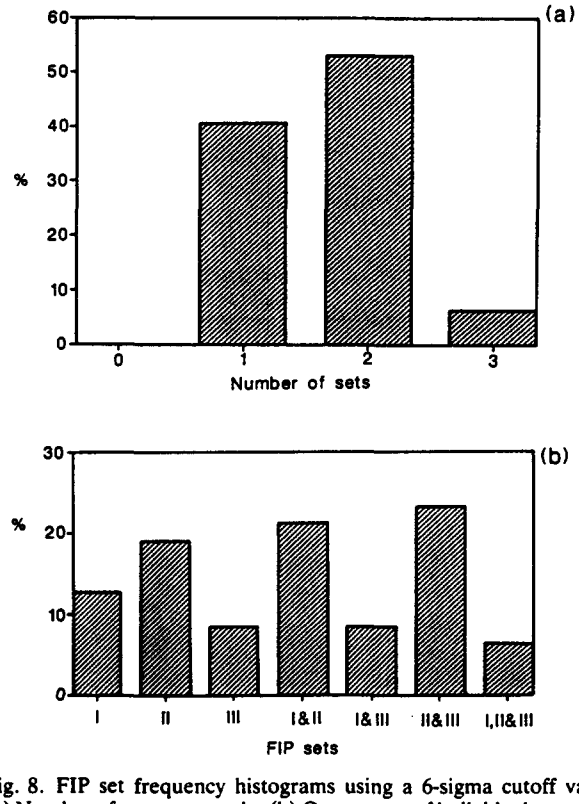

Fig. 8. FIP set frequency histograms using a 6-sigma cutoff value. (a) Number of sets per sample. (b) Occurrence of individual sets or set combinations.

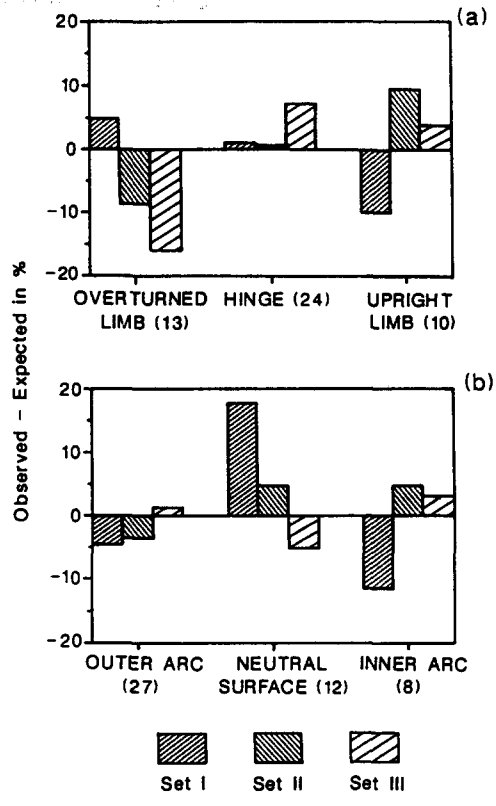

Fig. 9. Expected vs observed occurrence of three orthogonal FIP sets in Fig 7 at locations relative to (a) hinge and limbs, and (b) neutral surface of folding. Expected occurrence is a uniform distribution across the entire area which assumes that the proportions of the three FIP sets in any subarea will be the same as for the entire sample population. For all samples examined, the proportions are 49.0, 70.2 and 46.8% for sets I, II and III, respectively.

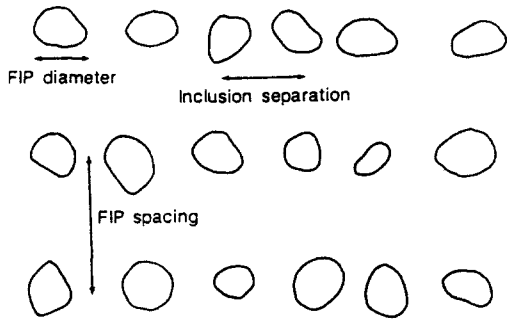

Fig. 10. Method used to determine extensional strain from FIPS. The three horizontal planes of inclusions shown correspond to three microfractures. In this example, extension from the three microfractures is 15%. See text for details of method.

variations during folding. However, simple relationships appear not to apply. Layer-parallel extension in outer arc regions during buckling or bending (Dietrich & Carter 1969) is thought to be the cause of strike-parallel veins in Lower Paleozoic carbonates of the Appalachian foreland (Srivastava & Engelder 1990). This explanation cannot be invoked for set III FIPS for two reasons: (1) they have the wrong orientation for layer-parallel extension in the limbs, where microfractures should be normal to layering (horizontal); and (2) they show no preferential development in outer arc samples compared to other FIP sets (Fig. 9b). It is possible that the Massanutten Sandstone behaved as multiple stiff layers with multiple neutral surfaces during folding, but the unit lacks evidence for multilayer behavior, such as bedding-parallel slip.

In summary, the FIPS formed predominantly in three orthogonal sets during folding. Set I FIPS formed either during the later stages of layer-parallel shortening (hinge) or during the later stages of folding by layer-parallel extension (limbs). Set II FIPS are Mode I cracks that formed in response to strike-parallel stretching during regional NW–SE compression, mostly during the early stages of folding. Set III FIPS formed in response to local stress conditions during folding.

MICROFRACTURES AND FINITE STRAIN

Although many studies point out the abundance of microfractures and their importance as a deformation mechanism (e.g. Mitra 1987), the contribution of microfractures to the finite strain has not been considered important. In the Massanutten Sandstone, pervasive microfracturing and elongation of grains normal to these microfractures (Figs. 5c & d) show that they do cause significant penetrative stretching.

Methodology

Seven samples were selected to determine the strain contribution of FIPS and microveins. They were chosen using two criteria: (1) they represent a range of microfracture development in the Massanutten Sandstone, from moderate to profuse; and (2) each mutually-perpendicular section is dominated by a single set of microfractures oriented at high angles to the section plane, thus simplifying the strain determination.

For comparison with microfracture strains, the finite strain in each section was determined using a normalized version of the Fry method (Fry 1979, Erslev 1988). In each of two separate areas on each section 150 grains were measured and the mean R_s for the slide computed.

The extension associated with the FIPS was determined assuming that the FIPS are healed extensional microfractures and that each FIP represents one microfracture. Using the average diameter of the inclusions and their average separation (Fig. 10) in an arbitrarily chosen 160 μm distance along the FIP, the total inclusion

Table 1. FIP density and microfracture strains. Volume increase for sample is sum of extensions from each different FIP set present. Sample notation is for mutually perpendicular thin sections:—1 = vertical and strike-normal;—2 = horizontal and strike-parallel; and—3 = vertical and strike-parallel

Sample	FIP set	FIPS (mm^{-1})	Extensional strain (%)			Volume increase (%) Total for sample
			FIPS	Microveins	Total	
MS28—1	Set III	31.3	3.2	2.4	5.6	
—2	Set III	57.0	6.1	1.3	7.4	16.4
—3	Set II	53.8	4.7	5.2	9.9	
MS68—1	Set III	75.6	5.5	0.7	6.2	
—2	Set II	78.8	4.5	1.4	6.9	12.6
—3	Set II	77.5	3.2	1.3	4.5	
MS78—1	Set III	55.0	2.3	3.9	6.2	
—2	Set III	87.5	5.5	2.2	7.7	12.5
—3	Set II	67.5	2.9	2.6	5.5	
MS79—1	Set I	89.4	4.4	0.3	4.7	
—2	Set II	15.0	0.4	0.2	0.6	5.2
—3	Set I	98.1	4.1	0.4	4.5	
MS165—1	Set III	62.5	4.2	0.9	5.1	
—2	Set II	136.3	6.2	0.4	6.6	11.0
—3	Set II	110.0	4.7	0.4	5.1	
MS188—1	None	0.0	0.0	0.0	0.0	
—2	Set II	168.0	6.1	5.0	11.1	9.4
—3	Set II	163.7	5.6	2.0	7.6	
MS196—1	Set I	111.9	7.0	3.4	10.4	
—2	Set II	58.8	2.6	1.1	3.7	12.7
—3	Set I	102.5	5.2	2.4	7.6	

area for each FIP can be calculated. Assuming that the total inclusion area along the FIP is equal to the area of the original microfracture, the width of microfracture is then calculated. From the microfracture widths and their spacing along a 160 μm distance normal to their trace (Fig. 10), the percent extension is found. Ten such determinations were made in each of two separate areas on each thin section and averaged for the mean percent extension (Table 1). Only the dominant set of FIPS was measured in each section (Table 1).

This method could overestimate the extensional strain by using inclusions that lie slightly out of the plane of focus. This potential error is offset by strain underestimation from the likelihood that the present inclusion volume is less than the original microfracture because microfractures may heal without trapping inclusions (Smith & Evans 1984). Underestimation would also result if the microfractures were sealed with material transported in from external sources rather than by local redistribution of material (healed). If this were the case, the inclusion area would represent only part of the original fracture area. Because of the rapid healing rates for narrow microfractures (<1.0 μm) (Evans & Charles 1977, Shelton & Orville 1980, Smith and Evans 1984), healing is believed to be the dominant closure process for FIPS.

The extensional strain from microveins was determined with cathodoluminescence. Each thin section contained one dominant set of microveins parallel to the FIPS (Figs. 5c and 6c). Traverses normal to this set were made across the entire section and the percent extension computed from the total width of microveins and the length of the traverse. Three traverses were made per section and the mean percent extension for the slide calculated (Table 1). This method assumes that the microveins were sealed with material external to the local area. Whereas healing would be favored by narrow microfractures, sealing would be more effective for wide microfractures (microveins).

Microfracture strains

In almost all samples, the FIPS account for more strain than the microveins (Table 1). Sections with abundant FIPS and microveins (e.g. MS188-2, Fig. 3) have extensional strains as great as 11.1%. Sections with only modest development of microfractures still record extensional strains of 4–7%. Because the method used to measure microfracture strains probably underestimates the extension, the actual extensions could be greater. Strains of this magnitude are significant, especially in quartz arenites of foreland regions, where XZ strain ratios of 1.1–1.5 are typical (Dunne *et al.* 1988).

No consistent relationship was found between the amount of strain and the three orthogonal FIP sets, although in many cases set II accounts for the highest strains. In general, this is due to set II having the greatest FIP densities.

The volume increase due to microfracturing was determined by summing the extensional strains from each microfracture set in the sample (Table 1). Where the same set appeared in two sections, the extensional strains for that set were averaged and added to the strain from the other set to yield the volume increase for the sample. The largest volume increase of 16.4% occurred in MS-28 (Fig. 3) which had two well developed sets of FIPS and microveins. Even though MS-188 had a higher single extension and greater FIP density (Table 1), it had a lower volume increase (9.4%) because it contained only one FIP set.

Table 2. Measured vs predicted microfracture strains. Predicted extension is calculated from strain ellipse determined by Fry method R_s assuming either constant-volume or volume-gain deformation. ϕ is the angle between the X-axis of finite strain ellipse and the extension direction of microfractures (normal to microfracture). Sample notation is same as Table 1

		Microfractures			Predicted e		% Predicted e explained by microfractures	
Sample	R_s	e	R	ϕ (°)	Constant-volume	Volume-gain	Constant-volume	Volume-gain
MS28—1	1.13	0.056	1.06	22	0.04	0.11	135.8	52.4
—2	1.36	0.074	1.07	6	0.16	0.35	46.0	20.9
—3	1.08	0.099	1.10	20	0.03	0.07	338.3	142.2
MS68—1	1.10	0.062	1.06	35	0.01	0.06	431.9	97.1
—2	1.12	0.069	1.07	20	0.04	0.10	160.9	66.5
—3	1.01	0.045	1.05	21	0.00	0.01	1218.6	517.3
MS78—1	1.09	0.062	1.06	10	0.04	0.09	150.9	71.3
—2	1.30	0.077	1.08	6	0.14	0.30	56.7	26.1
—3	1.21	0.055	1.06	35	0.02	0.13	227.6	44.0
MS79—1	1.45	0.047	1.05	1	0.20	0.45	23.0	10.5
—2	1.57	0.006	1.01	2	0.25	0.57	2.4	1.1
—3	1.24	0.045	1.05	3	0.11	0.24	40.0	18.9
MS165—1	1.22	0.051	1.05	20	0.07	0.19	68.7	27.3
—2	1.14	0.066	1.07	2	0.07	0.14	97.8	47.2
—3	1.12	0.051	1.05	14	0.05	0.11	101.0	45.6
MS188—1	1.26	0.000	1.00	N/A	0.08	0.21	0.0	0.0
—2	1.30	0.111	1.11	5	0.14	0.30	80.9	37.4
—3	1.30	0.076	1.08	3	0.14	0.30	54.6	25.4
MS196—1	1.27	0.104	1.10	4	0.13	0.27	83.0	38.8
—2	1.17	0.037	1.04	6	0.08	0.17	46.6	22.1
—3	1.40	0.076	1.08	16	0.14	0.35	53.4	21.6

The contribution of microfractures to the finite strain can be assessed in several ways. The angle (ϕ, Table 2) between the X-axis of the finite strain ellipse and the normal to the microfracture set (extension direction) is one measure of this contribution. If all finite strain was due to microfracturing, ϕ would be zero. A non-zero angle indicates that other mechanisms were operative in a non-coaxial fashion or that the angle was affected by depositional fabrics. ϕ is always less than 35° and averages 5.5° which shows that microfractures contribute greatly to the finite strain.

Another way of assessing the microfracture strain is by using the finite strain ellipse (R_s, Table 2) to calculate the extension in a direction normal to the microfractures. By comparing this calculated extension to the measured microfracture extension, the contribution of the microfractures to the finite strain can be evaluated.

Two end-member cases were considered (Table 2): (1) constant-volume deformation where volume gains associated with microfracturing are offset by volume loss from mechanisms such as pressure solution; and (2) volume-gain deformation, as would be the case for microfracturing alone. For both cases, a value less than 100% indicates that microfractures cannot fully account for finite extension normal to their trace. A value greater than 100% indicates that the microfracture strains exceed the finite extension in that direction. This could be due to non-coaxial deformation with a component of shortening normal to the microfractures. As such, it is a measure of importance of other deformation mechanisms like pressure solution or dislocation flow.

For the constant-volume case, the microfracture extensions account for much of the strain, but exceed the finite extensions in 38% of the sections (Table 2). For the volume-gain case, less of the strain is accounted for by microfractures, but the finite extension is exceeded in only 10% of the sections. These data show that the deformation was neither constant-volume nor volume-gain. For volume-gain deformation, the values greater than 100% are an indication that deformation mechanisms other than microfracturing contributed to the finite strain. This is consistent with the presence of microstructures such as deformation lamellae and seams of insoluble residue in some samples. Many samples, however, lack microstructures indicative of shortening to counteract the dilation from the microfractures. Thus, it is likely that deformation resulted in a net volume gain.

DISCUSSION

In the Massanutten Sandstone, microfracturing was the dominant deformation mechanism. Yet, the abundance of microfractures, especially FIPS, is surprising. The density of microfractures is very high when compared to previously reported values for both naturally and experimentally deformed rocks. Blenkinsop & Rutter (1986) found microfracture densities of 5.7–36 mm^{-1} in quartzite cataclasites of the Moine thrust zone. Experimentally deformed samples of Westerly granite have densities in the range of 4.9–23.5 mm^{-1} (Friedman & Logan 1970, Tapponier & Brace 1976). Densities in the Massanutten Sandstone exceed these values by several times.

The exceedingly high microfracture densities in the Massanutten Sandstone raise two questions: (1) why did the large number of microfractures not lead to cataclastic failure; and (2) why did microfractures not propagate unstably to become large joints? Several workers have proposed that a critical crack density is necessary for cataclastic failure (Scholz 1968a, Kranz & Scholz 1977, Costin 1983). For example, Blenkinsop & Rutter (1986) found that an increase in the density of extensional microfractures correlated with the progressive brecciation and development of cataclasite in the Moine thrust zone. The high microfracture densities and lack of cataclastic textures in the Massanutten Sandstone indicate that if such a threshold density is necessary for cataclasis, it must be much higher than previously believed or that other factors are involved. Chief among these is the rate at which the microfractures are closed. It appears that the microfractures in the Massanutten Sandstone closed rapidly enough so that at any one time, the number of open microfractures was low and that the critical 'active' density was never achieved. Rapid healing is supported by experiments of Smith & Evans (1984) who found that, in the presence of water, microfractures heal in only several hours at 400°C. At 200°C, which is similar to conditions during deformation of the Massanutten Sandstone, they predicted that microfractures would have geologically short lifetimes.

The propagation and subsequent linking of microfractures has been shown to be important in process zones of joints (Friedman *et al.* 1972). In the Massanutten Sandstone, propagation could have been stopped by grain boundaries acting as elastic discontinuities. However, grain-boundary discontinuities in a quartz-cemented, quartz arenite would be small and would have little effect on the mechanical behavior of the rock (Gallagher *et al.* 1974). A second and more likely explanation for the failure of microfractures to propagate is rapid closure.

The rapid healing of microfractures requires that pore fluids be present (Smith & Evans 1984). Insight into the pore fluid pressure during microfracturing in the Massanutten Sandstone is provided by the nature of the microfractures. Intragranular microfractures will tend to form where grain boundaries acts as stress risers (Gallagher *et al.* 1974). Microfracturing can proceed at low stresses without the need for high pore fluid pressures. In the Massanutten Sandstone, grain boundaries have minimal significance and would not have acted as stress risers. This, along with the abundance of transgranular microfractures (transgranular FIPS and microveins), argues that pore fluid pressures must have been high. These conditions are similar to those proposed by Lacazette & Engelder (1987) for the Bald Eagle and Juniata sandstones in Pennsylvania which are largely correlative with the Massanutten Sandstone.

Of great importance for deformation analysis of fore-

land sandstones is the potential volume increase from microfracturing. The importance of volume loss during deformation is well known (Ramsay & Wood 1973, Wood 1974), but much less is known about volume increases. A problem in any volume-loss deformation is finding a sink for the dissolved material. Microfractures provide such a sink for material derived locally or from adjacent areas. Shales in the Martinsburg Formation, which directly underlie the Massanutten Sandstone, have suffered up to 50% volume loss during cleavage formation (Wright & Platt 1982). The sink for this material is partly within the unit (Woodward *et al.* 1986); however, the proximity of the Massanutten Sandstone and the abundance of closed microfractures suggests that the sandstone may have provided an additional sink for material lost from the Martinsburg Formation.

CONCLUSIONS

Microfracturing was the dominant deformation mechanism in much of the Massanutten Sandstone. Microfractures in the form of fluid inclusion planes and microveins formed during folding and resulted in extensional strains as high as 11% and volume increases of up to 17%. These strains are significant, especially in a foreland setting. Failure to consider them could result in a major portion of the finite strain being erroneously attributed to other mechanisms.

The exceedingly high microfracture density in the Massanutten Sandstone did not result in brecciation or unstable fracture propagation suggesting that the high rate of healing is important in suppressing the development of cataclastic textures and long joints. The strong possibility of a net volume increase in the sandstone indicates that this unit may have provided a sink for material from other units undergoing volume-loss deformation.

Acknowledgements—William Dunne helped clarify the role of microfractures in folding. Discussions with Richard Groshong, Jr, led to the method for determining strain from FIPS. Their comments on early drafts of this paper were very helpful. Reviews by Stephen Laubach and Terry Engelder are appreciated. This work was supported by NSF grant EAR-8500389 to the author.

REFERENCES

Allen, R. M., Jr. 1967. Geology and mineral resources of Page County. *Bull. Virginia Div. Miner. Resour.* **81**.

Anderson, E. M. 1951. *The Dynamics of Faulting and Dyke Formation, With Applications to Britain*. Oliver and Boyd, London.

Berger, P. S., Perry, W. J., Jr. & Wheeler, R. L. 1979. Three-stage model of brittle deformation in the central Appalachians. *Southeastern Geol.* **20**, 59–67.

Blenkinsop, T. G. & Rutter, E. H. 1986. Cataclastic deformation of quartzite in the Moine thrust zone. *J. Struct. Geol.* **8**, 669–681.

Costin, L. S. 1983. A microcrack model for the deformation and failure of brittle rock. *J. geophys. Res.* **88**, 9485–9492.

Dietrich, J. H. & Carter, N. L. 1969. Stress history of folding. *Am. J. Sci.* **267**, 124–154.

Dula, W. F. 1981. Correlation between deformation lamellae, microfractures, macrofractures, and *in situ* stress measurements, White River Uplift, Colorado. *Bull. geol. Soc. Am.* **92**, 37–46.

Dunne, W. M., Billman, D. A., Johnston, M. A., Rohaus D. & Gerritsen, S. 1988. Cover deformation above foreland thrust systems and strains in sandstones. *Geol. Soc. Am. Abs. w. Prog.* **20**, A57.

Engelder, T. 1974. Cataclasis and the generation of fault gouge. *Bull. geol. Soc. Am.* **85**, 1515–1522.

Engelder, T. 1984. The time-dependent strain relaxation of Algerie granite. *Int. J. Rock Mech. Min. Sci. Geomech. Abs.* **21**, 63–73.

Engelder, T. & Geiser, P. A. 1980. On the use of regional joint sets as trajectories of paleostress fields during the development of the Appalachian Plateau, New York. *J. geophys. Res.* **85**, 6319–6341.

Epstein, R. L. 1988. Illite crystallinity of the Middle and Upper Ordovician allochthonous and autochthonous rocks in the Great Valley of central Pennsylvania. Unpublished M.Sc. thesis, Bowling Green State University, Ohio.

Erslev, E. 1988. Normalized center-to-center strain analysis of packed aggregates. *J. Struct. Geol.* **10**, 201–209.

Evans, M. 1989. The structural geometry and evolution of foreland thrust systems, northern Virginia. *Bull. geol. Soc. Am.* **101**, 339–354.

Evans, A. G. & Charles, E. A. 1977. Strength recovery by diffusive crack healing. *Acta metall.* **25**, 919–927.

Friedman, M. & Logan, J. M. 1970. Microscopic feather fractures. *Bull. geol. Soc. Am.* **81**, 3417–3420.

Friedman, M. Handin, J. & Alani, G. 1972. Fracture energy of rocks. *Int. J. Rock Mech. Min. Sci.* **9**, 757–766.

Fry, N. 1979. Random point distributions and strain measurement in rocks. *Tectonophysics* **60**, 89–105.

Gallagher, J. J., Friedman, M., Handin, J. & Sowers, G. M. 1974. Experimental studies relating to microfracture in sandstones. *Tectonophysics* **21**, 203–247.

Groshong, R. H., Jr. 1988. Low temperature deformation mechanisms and their interpretation. *Bull. geol. Soc. Am.* **100**, 1329–1360.

Haimson & Doe, T. W. 1983. State of stress, permeability, and fractures in the Precambrian granite of northern Illinois. *J. geophys. Res.* **88**, 7355–7371.

Hobbs, B. E., Means, W. D. & Williams, P. F. 1976. *An Outline of Structural Geology*. John Wiley, New York.

Kamb, B. 1959. Ice petrofabric observations from Blue Glacier, Washington, in relation to theory and experiment. *J. geophys. Res.* **64**, 1891–1909.

Kowallis, B. J., Wang, H. F. & Jang, B. 1987. Healed microcrack orientations in granite from Illinois borehole UPH-3 and their relationship to the rock's stress history. *Tectonophysics* **135**, 297–306.

Kranz, R. L. 1983. Microcracks in rocks: a review. *Tectonophysics* **100**, 449–480.

Kranz, R. L. & Scholz, C. H. 1977. Critical dilatant volume of rocks at the onset of tertiary creep. *J. geophys. Res.* **82**, 4893–4897.

Lacazette, A. & Engelder, T. 1987. Reducing fluids and the origin of natural fractures in the Bald Eagle Sandstone, Pennsylvania. *Geol. Soc. Am. Abs. w. Prog.* **19**, 737.

Laubach, S. E. 1989. Paleostress directions from the preferred orientation of closed microfractures (fluid inclusion planes) in sandstone, East Texas basin, U.S.A. *J. Struct. Geol.* **11**, 603–612.

Lespinasse, M. & Pêcher, A. 1986. Microfracturing and regional stress field: a study of the preferred orientation of fluid-inclusions planes in a granite from the Massif Central, France. *J. Struct. Geol.* **8**, 169–180.

Marshall, D. J. 1988. *Cathodoluminescence of Geological Materials*. Unwin Hyman, Boston.

Mitra, S. 1987. Regional variations in deformation mechanisms and structural styles in the central Appalachian orogenic belt. *Bull. geol. Soc. Am.* **98**, 569–590.

Narahara, D. K. & Wiltschko, D. V. 1986. Deformation in the hinge region of a chevron fold, Valley and Ridge Province, central Pennsylvania. *J. Struct. Geol.* **8**, 152–168.

Onasch, C. M. 1984. Petrofabric test of viscous buckling theory. *Tectonophysics* **106**, 141–153.

Onasch, C. M. 1987. Microfractures and the deformational history in a portion of the central Appalachian Great Valley. *Geol. Soc. Am. Abs. w. Prog.* **19**, 794.

Pêcher, A., Lespinasse, M. & Leroy, J. 1985. Relations between fluid inclusion trails and regional stress field: a tool for fluid chronology—an example of an intragranitic uranium ore deposit (northwest Massif Central, France). *Lithos* **18**, 229–237.

Plumb, R., Engelder, T. & Yale, D. 1984. Near-surface *in situ* stress: correlation with microcrack fabric within the New Hampshire granites. *J. geophys. Res.* **89**, 9350–9364.

Price, R. A. 1967. The tectonic significance of mesoscopic subfabrics in the southern Rocky Mountains of Alberta and British Columbia. *Can. J. Earth Sci.* **4**, 39–70.

Rader, E. K. & Biggs, T. H. 1976. Geology of the Strasburg and Toms Brook quadrangles, Virginia. *Virginia Div. Min. Resour. Rep. Invest.* **45**.

Ramsay, J. G. & Huber, M. I. 1987. *The Techniques of Modern Structural Geology, Volume 2: Folds and Fractures*. Academic Press, London.

Ramsay, J. G. & Wood, D. S. 1973. The geometric effects of volume change during deformation processes. *Tectonophysics* **16**, 263–277.

Scholz, C. H. 1968a. Microfracturing and the inelastic deformation of rock in compression. *J. geophys. Res.* **73**, 1417–1432.

Scholz, C. H. 1968b. An experimental study of the fracturing process in brittle rock. *J. geophys. Res.* **73**, 1447–1454.

Shelton, K. L. & Orville, P. M. 1980. Formation of synthetic fluid inclusions in natural quartz. *Am. Miner.* **65**, 1233–1236.

Simmons, G. & Richter, D. 1976. Microcracks in rocks. In: *The Physics and Chemistry of Minerals and Rocks* (edited by Sterns, R. J. G.). Wiley-Interscience, New York, 105–137.

Smith, D. L. & Evans, B. 1984. Diffusional crack healing in quartz. *J. geophys. Res.* **89**, 4125–4135.

Sprunt, E. S. & Nur, A. 1979. Microcracking and healing in granites: new evidence from Cathodoluminescence. *Science* **205**, 495–497.

Srivastava, D. C. & Engelder, T. 1990. Crack-propagation sequence and pore-fluid conditions during fault-bend folding in the Appalachian Valley and Ridge, central Pennsylvania. *Bull. geol. Soc. Am.* **102**, 116–128.

Stearns, D. W. 1968. Certain aspects of fracture in naturally deformed rocks. In: *NSF Advanced Science Seminar in Rock Mechanics* (edited by Riecker, R. E.). Bedford, Massachusetts, Air Force Cambridge Research Laboratories Special Report, 97–118.

Tapponier, P. & Brace, W. F. 1976. Development of stress induced microcracks in Westerly Granite. *Int. J. Rock Mech. Sci.* **13**, 103–112.

Tuttle, O. F. 1949. Structural petrology of planes of liquid inclusions. *J. Geol.* **57**, 331–356.

Wang, H. F. & Simmons, G. 1978. Microcracks in crystalline rock from 5.3 km depth in the Michigan basin. *J. geophys. Res.* **83**, 5849–5856.

Wise, D. U. 1964. Microjointing in basement, Middle Rocky Mountains of Montana and Wyoming. *Bull. geol. Soc. Am.* **75**, 287–306.

Wood, D. S. 1974. Current views of the development of slaty cleavage. *Annu. Rev. Earth Sci.* **2**, 1–35.

Woodward, N. B., Gray, D. R. & Spears, D. B. 1986. Including strain data in balanced cross-sections. *J. Struct. Geol.* **8**, 313–324.

Wright, T. O. & Platt, L. B. 1982. Pressure dissolution and cleavage in the Martinsburg Shale. *Am. J. Sci.* **282**, 122–135.